

# Structural Characterization of U(VI) in Apatite by X-ray Absorption Spectroscopy

JOHN RAKOVAN,<sup>\*,#</sup> RICHARD J. REEDER,<sup>†</sup>  
 EVERT J. ELZINGA,<sup>†</sup>  
 DANIELE J. CHERNIAK,<sup>‡</sup>  
 C. DREW TAIT,<sup>§</sup> AND DAVID E. MORRIS<sup>§</sup>

Department of Geology, Miami University,  
 Oxford, Ohio 45056, Department of Geosciences, State  
 University of New York, Stony Brook, New York 11794-2100,  
 Department of Earth & Environmental Sciences, Rensselaer  
 Polytechnic Institute, Troy, New York 12180, and  
 Chemistry Division and the Glenn T. Seaborg Institute for  
 Transactinium Science, Los Alamos National Laboratory,  
 Los Alamos, New Mexico 87545

X-ray absorption spectroscopy was used to determine the local structure of U(VI) within synthetic fluorapatite at a concentration of 2.3 wt %. Extended X-ray absorption fine structure indicates that U(VI) substitutes into the Ca1 site. To accommodate this substitution the apatite structure significantly distorts such that the Ca1 site approximates octahedral coordination, with six uniform U–O distances of 2.06 Å. An X-ray adsorption edge structure, with two inflection points, and optical emission spectra are consistent with 6d orbital crystal field splitting. These results indicate that significant amounts of U(VI) can be accommodated in the apatite structure but with an unexpected coordination, which may bear on the ultimate development of apatite-hosted nuclear-waste forms.

## Introduction

Apatite,  $\text{Ca}_{10}(\text{PO}_4)_6(\text{F},\text{OH},\text{Cl})_2$ , forms extensive solid solutions among F, OH, and Cl, with the F-rich end-member being most common in nature (1). Its structure can also accommodate numerous other elemental substitutions, including many radionuclides of environmental concern (1). Uranium concentrations in natural apatites are commonly in the parts per million range but can reach a few weight percent (2, 3). Uranium in apatite has been used extensively in geochronologic and petrogenetic studies for over half a century (4). Furthermore, because of its high affinity for U and other radionuclides (1) and its thermal annealing behavior (5–8), there is great interest in apatite as a solid nuclear-waste form (9–12) and an engineered contaminant barrier (13, 14). Fluorapatite is one of the most radiation-damage resistant materials at temperatures above 70 °C and hence is of particular interest in these applications (9–12). Fundamental to our understanding of radionuclide retention and release are crystal chemical parameters such as site occupancy, oxidation state, and structural distortions created by substituents. Despite the interest in U in apatite, the basic crystal

\* Corresponding author phone: (513)529-3245; fax: (513)529-1542; e-mail: Rakovajf@muohio.edu.

# Miami University.

† State University of New York.

‡ Rensselaer Polytechnic Institute.

§ Los Alamos National Laboratory.

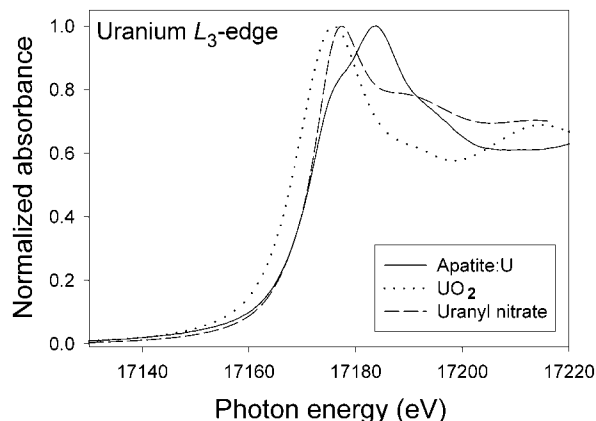


FIGURE 1. Room-temperature U  $L_3$  XANES data from apatite,  $\text{U}^{4+}\text{O}_2$ , and uranyl nitrate hexahydrate.

chemistry of its substitution in the structure is still unknown. In this study X-ray absorption spectroscopy (XAS) and corroborative optical spectroscopies were used to determine local structure of U(VI) within fluorapatite. We present the first direct evidence of the site of incorporation and the response of the structure to this substituent.

## Experimental Methods

**Sample Synthesis.** A powder sample of U-rich fluorapatite,  $\text{Ca}_{9.9}\text{U}_{0.1}(\text{PO}_4)_6\text{F}_{1.8}$ , was synthesized from stoichiometric proportions of  $\text{UO}_2$ ,  $\text{Ca}_3(\text{PO}_4)_2$ , and  $\text{CaF}_2$ . The procedures are adapted from the work of Kriedler and Hummel (15). The starting material was ground and annealed at  $\sim 1380$  °C for 1–2 days in a Pt capsule open to air. Under these oxidizing conditions the U(IV) readily oxidizes to U(VI). Powder X-ray diffraction showed that the final product is fluorapatite (see Figure 1, Supporting Information).

**X-ray Absorption Spectroscopy (XAS).** XAS was conducted at the X18B beamline of the National Synchrotron Light Source, Brookhaven National Laboratory, U.S.A. The storage ring operated at 2.8 GeV with a maximum current of 280 mA. All XAS spectra were collected at the U  $L_3$ -edge using a Si(111) channel-cut monochromator, detuned by 20% to reduce harmonics. The monochromator was calibrated using  $\text{UO}_2$  and uranyl nitrate hexahydrate as U(IV) and U(VI) reference samples. The first peak in the derivative of the uranyl nitrate spectrum was assigned the energy 17 171 eV. Spectra were collected from the apatite in fluorescence mode, using a passivated implanted planar silicon (PIPS) detector positioned at 90° to the incident beam, and from model compounds in transmission mode using ion chambers. Sixteen scans were collected at room temperature and averaged to obtain the raw spectrum for EXAFS fitting. A preedge linear background and a postedge second-order polynomial were used for normalization. The  $\chi(k)$  was extracted using a cubic spline and Fourier transformed with  $k^3$  weighting. EXAFS fitting was done in  $R$  space with the program WinXAS (16), using theoretical phases and amplitudes calculated by FEFF7 (17). Starting models for FEFF calculations included U positioned at both the Ca1 and Ca2 sites in fluorapatite. All fit parameters were allowed to vary except the coordination numbers of shells located beyond the first oxygen shell; these were fixed at values consistent with U substitution in the respective Ca site. A global  $E_0$  was allowed to vary during fitting, and the total number of fit parameters varied never exceeded the limit constrained by the  $k$  and  $R$  space ranges (2.1–14.8 Å<sup>-1</sup> and 0.3–4.6 Å,

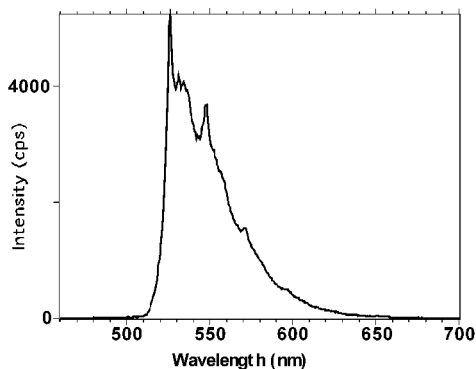


FIGURE 2. Luminescence spectrum at liquid nitrogen temperature, using 400 nm excitation.

respectively). Estimated errors are  $\pm 15\%$  for coordination number,  $\pm 0.02 \text{ \AA}$  for first-shell distances and  $\pm 0.03 \text{ \AA}$  for more distant shells, and  $\pm 0.002 \text{ \AA}^2$  for Debye–Waller type parameters. XANES spectra were collected with simultaneous calibration relative to either the uranyl nitrate or  $\text{UO}_2$  reference sample.

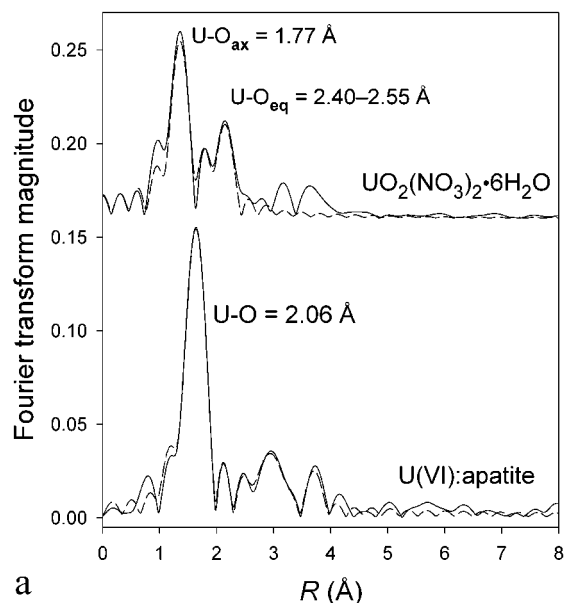
**Luminescence and Diffuse Reflectance.** Optical luminescence (18, 19) and diffuse reflectance (20) data were collected for independent determination of the U oxidation state. Time-resolved luminescence spectra were collected using a SPEX Industries Fluorolog 2 system. Data were collected at liquid nitrogen temperature, using 400 nm excitation.

## Results and Discussion

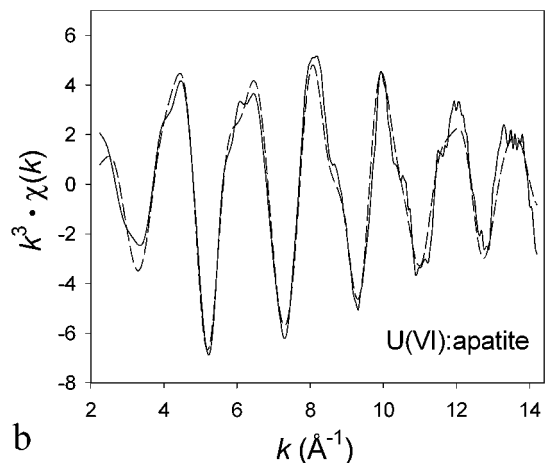
The XANES spectrum (Figure 1) shows an unexpected structure in the  $U L_3$  absorption edge. Reference materials exhibit characteristic edge shapes with a 1–2 eV shift between U(IV) and U(VI). For the U-apatite there are two inflection points in the edge. The first inflection point coincides with the inflection point in the absorption edge in uranyl nitrate. However, the second inflection point is 8.4 eV higher, and the absorption maximum is shifted approximately 6 eV higher relative to that in uranyl nitrate, making this latter feature in the edge unsuitable for determination of the uranium oxidation state.

To independently determine the oxidation state of U, optical luminescence (18, 19) and diffuse reflectance (20) data were collected. A strong emission spectrum at liquid-nitrogen temperature with 400 nm excitation was obtained (Figure 2) and indicates the presence of uranium in the 6+ oxidation state. A single-exponential lifetime of 145  $\mu\text{s}$  throughout the spectral region of the main luminescence (526, 535, and 548 nm) suggests that it is from a single species (21). However, this spectrum does not show the typical vibronic characteristics of a dioxo-uranyl species. Lack of oxidation-state-characteristic peaks in the red and near-infrared diffuse reflectance, moreover, shows that there is no significant U(IV) or U(V) in the sample (20). These results combined with the observed XANES spectra indicate that the vast majority of the U is hexavalent.

The apatite U(VI) EXAFS spectrum, Fourier transform modulus (uncorrected for phase shift), and best fit are shown in Figure 3. In the  $P6_3/m$  apatite structure there are three cation sites: the tetrahedral P site and two nonregular Ca sites (Ca1 and Ca2). The Ca1 site is coordinated to nine O atoms and has point symmetry 3 [equipoint 4(f)]. Three O1 atoms and three O2 atoms form a twisted, trigonal prism with Ca–O distances of 2.399(2)  $\text{\AA}$  and 2.457(2)  $\text{\AA}$ , respectively (22). Three O3 atoms lie around the midsection of the trigonal prism with a much longer Ca–O bond length of 2.807(2)  $\text{\AA}$  (Figure 4a). The Ca2 site is coordinated to six O atoms and one column anion (F, OH, or Cl), with point symmetry  $m$



a



b

FIGURE 3. (a) Fourier transform magnitudes (not corrected for phase shifts) of U(VI) in synthetic fluorapatite and the uranyl nitrate hexahydrate reference compound with best fits shown by dashed lines. The higher magnitude of the U–O peak in the U(VI):apatite reflects six oxygens at a single distance. (b) The  $k^2$  weighted EXAFS with best fit (dashed line).

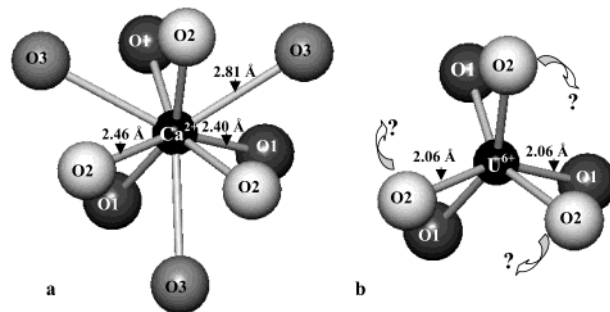


FIGURE 4. (a) Geometry of the Ca1 site in fluorapatite viewed down [001] with bond distances indicated. (b) Experimentally determined U–O distance and speculated distortion of the Ca1 site occupied by U(VI).

[equipoint 6(h)]. Ca2-anion bond distances are 2.701(1)  $\text{\AA}$  for O1, 2.374(2)  $\text{\AA}$  for O2, 2.349(3)  $\text{\AA}$  and 2.501(3)  $\text{\AA}$  for the O3 atoms, and 2.3108(7)  $\text{\AA}$  for F (22). The EXAFS fitting results are consistent with U(VI) substitution into the Ca1 sites, based

TABLE 1. EXAFS Fitting Parameters<sup>a</sup>

	O shell	P shell	Ca shell	P shell	Ca shell	O shell
<i>N</i>	6.0	3 <sup>b</sup>	2 <sup>b</sup>	3 <sup>b</sup>	6 <sup>b</sup>	6 <sup>b</sup>
<i>R</i> (Å)	2.06	3.19	3.39	3.58	4.02	4.06
<i>σ</i> <sup>2</sup> (Å <sup>2</sup> )	0.003	0.016	0.007	0.006	0.012	0.003

<sup>a</sup> *N* = coordination number, *R* = distance from the U ion, *σ*<sup>2</sup> = Debye–Waller factor. Error estimates in the radial distances found in the fitting procedure are ± 0.02 Å for the first shell, and ± 0.03 Å for higher shells, based on fits of experimental spectra of well-characterized U reference compounds. Radial distances for the Ca1 and Ca2 sites of pure fluorapatite are tabulated in Table 1 of Supporting Information. <sup>b</sup> Fixed at values of Ca1 site.

on the strong similarity in the radial distances of the shells surrounding Ca1, with the exception of the first shell O distance (Table 1). Attempts to fit the data assuming U(VI) substitution in the Ca2 sites failed: the quality of the fit drastically decreased, and the optimized radial distances deviated strongly from those of the shells surrounding Ca2 in apatite. The EXAFS fit shows, however, almost all the expected shells for substitution of U(VI) in the Ca1 site of apatite, except for a weak or absent contribution from the O3 shell; a U(VI)–O3 correlation is unidentifiable. The Fourier transform is dominated by a single peak corresponding to the first shell, that was best fitted with  $6 \pm 1$  oxygen atoms at 2.06 Å, with a small Debye–Waller factor ( $\sigma^2 = 0.003 \text{ \AA}^2$ ). The single oxygen shell differs markedly from the usual coordination of U(VI) by two axial oxygens at ~1.8 Å and 4–6 equatorial oxygens at 2.25–2.45 Å, as shown by the uranyl nitrate reference material (Figure 3a). The single O shell at 2.06 Å agrees very well with reported U(VI)–O distances found in structures having U(VI) in holosymmetric octahedral coordination: 2.05–2.09 Å in Ca<sub>3</sub>UO<sub>6</sub> (23), 2.07–2.10 Å in Sr<sub>3</sub>UO<sub>6</sub> (24), and 2.08 Å in δ-UO<sub>3</sub> (25).

With the local structure around U determined from the EXAFS, the XANES and luminescence spectra can be re-examined in more detail. The similarity in the structure of the X-ray absorption edge to the *L*<sub>3</sub> absorption edge of U(VI) in synthetic Ba<sub>2</sub>ZnUO<sub>6</sub> (perovskite structure) (26) is striking. For Ba<sub>2</sub>ZnUO<sub>6</sub>, U(VI) was determined to be in a regular octahedral site with cubic symmetry, suggesting the possibility of such an environment around U(VI) in apatite. The U–O distance in Ba<sub>2</sub>ZnUO<sub>6</sub> (2.09 Å) (26) is very close to the value we find 2.06 Å. The absorption edge found in apatite suggests that the crystal field may play a role in the structure of the edge, which must be considered when using XANES for the determination of U oxidation in materials. Den Auwer et al. (26) conclude that this edge structure is due to a crystal field splitting of the U 6d orbitals, leading to two *L*<sub>3</sub> transitions ( $2p_{3/2} \rightarrow 6d t_{2g}$  and  $2p_{3/2} \rightarrow 6d e_g$ ). Furthermore, the luminescence spectrum of the U(VI):apatite and its vibronic structure are quite similar to those reported for the octahedral UO<sub>6</sub><sup>6-</sup> moiety (27), with the main progression corresponding to  $\nu_1 \sim 755 (\pm 20) \text{ cm}^{-1}$ . The similarity of the apatite XANES and luminescence spectra to those of structures with octahedrally coordinated U further supports the octahedral ligation of U in apatite (26, 27).

The octahedral coordination around U(VI) in apatite is quite surprising, given that U(VI) in minerals has previously been found only as part of the near linear uranyl ion, and known uranium(VI) phosphates contain the dioxo configuration exclusively. The bond valence sum for U(VI) in 6-fold coordination with the observed distance of 2.06 Å, calculated using newly refined bond valence constants (28), is 5.9. This is very close to the formal charge on the uranium ion and further suggests a very weak, if any, bonding contribution from the O3 ions normally associated with the Ca1 site. Furthermore, movement of the O3 ions away from the Ca1 site, toward Ca2 would help compensate for the reduction

in bond valence around Ca2 created by shortening of the O1–U and O2–U bond distances. The significant shortening of the U–O bonds relative to the Ca–O1 and Ca–O2 bonds in apatite bring the O1 and O2 atoms closer together. These two effects must lead to further distortions in the apatite structure that are not revealed in the EXAFS data. One likely distortion is the rotation of the O1 and O2 triads to form a more regular octahedral geometry around the U(VI) (Figure 4b). Also, the Debye–Waller factor of the fitted P shell in the EXAFS data is relatively high, suggesting a high degree of variance in the distance between U and the first nearest neighbor P ions surrounding the Ca1 site. This should be expected since the rigid PO<sub>4</sub> tetrahedra coordinating with the U(VI) must be displaced relative to their positions in ideal fluorapatite.

One of the most pressing environmental problems facing society today is the containment and disposal of radioactive wastes. Apatite has been identified as one of the most promising phases for the long-term isolation of high levels of several radionuclides, including uranium (9–12, 29), and a great deal of research is being conducted in France, the United States, and elsewhere to fully assess this potential. It is shown here that fluorapatite can accommodate large concentrations of U(VI), and the substitution of this ion leads to a unique distortion of the structure creating a near octahedral coordination. It is interesting to note that the site geometry of U(VI) in apatite is similar to that in other structures, i.e., perovskites, being considered as solid waste forms (30–32). The stability of fluorapatite with high loadings of U(VI) has yet to be determined. However, if the distortion around U(VI) has a stabilizing effect it may make this the optimal oxidation state for long-term containment. The fundamental crystal chemistry of U(VI) presented here is essential to the ultimate development of apatite solid nuclear-waste forms and is of great interest for geochronologic and trace element studies of natural samples.

### Acknowledgments

This work was supported by NSF grant EAR 9814691, DOE grant DE-FG07-99ER15013, and the Office of Basic Energy Sciences, U.S. DOE, under Contract W-7405-ENG-36 with the University of California. We thank the beamline staff at X18B (NSLS).

### Supporting Information Available

A powder X-ray diffraction pattern of the U(VI) doped fluorapatite used in this study and a table of the radial distances out to approximately 4 Å for the Ca1 and Ca2 sites of U-free fluorapatite. This material is available free of charge via the Internet at <http://pubs.acs.org>.

### Literature Cited

- (1) Elliott, J. C. *Structure and Chemistry of the Apatites and other Calcium Orthophosphates*; Elsevier: Amsterdam, 1994.
- (2) Jerden, J. L., Jr.; Beard, J.; Sinha, A. K. *Abstr. Prog. – Geol. Soc. Am.* **1998**, *30*, 182.
- (3) Altschuler, Z. S.; Clarke, R. S., Jr.; Young, E. J. *U.S. Geol. Sur. Prof. Pap.* **1958**, *1–90*.
- (4) McConnell, D. *Apatite; its Crystal Chemistry, Mineralogy, Utilization and Geologic and Biologic Occurrences*; Springer-Verlag: New York, 1973.
- (5) Soulet, S.; Chaumont, J.; Krupa, J.-C.; Carpena, J.; Ruault, M.-O. *J. Nucl. Mater.* **2001**, *289*, 194.
- (6) Weber, W. J.; Ewing, R. C.; Meldrum, A. *J. Nucl. Mater.* **1997**, *250*, 147.
- (7) Meis, C.; Gale, J. D.; Boyer, L.; Carpena, J.; Gosset, D. *J. Phys. Chem. A* **2000**, *104*, 5380.
- (8) Bros, R.; Carpena, J.; Sere, V.; Beltritti, A. *Radiochim. Acta* **1996**, *74*, 277.
- (9) Ewing, R. C. *Proc. Natl. Acad. Sci.* **1999**, *96*, 3432.
- (10) Ewing, R. C. *Can. Min.* **2001**, *39*, 697.
- (11) Carpena, J.; Lacout, J. L. France Patent 93 08676, 1993.

- (12) Carpena, J.; Boyer, L.; Lacout, J. L. France Patent 98 11334, 1998.
- (13) Jeanjean, J.; Rouchaud, J. C.; Tran, L.; Fedoroff, M. *J. Radioanal. Nuc. Chem., Lett.* **1995**, *201*, 529.
- (14) Arey, J. S.; Seaman, J. C.; Bertsch, P. M. *Environ. Sci. Technol.* **1999**, *33*, 337.
- (15) Kriedler, E. R.; Hummel, F. A. *Am. Min.* **1970**, *55*, 170.
- (16) Ressler, T. *J. Physiq.* **1997**, *IV*, C2.
- (17) Zabinsky, S. I.; Rehr, J. J.; Ankudinov, A.; Albers, R. C.; Eller, M. *J. Phys. Rev.* **1995**, *B52*, 2995.
- (18) Clark, D. L.; Conradson, S. D.; Donohoe, R. J.; Keogh, D. W.; Morris, D. E.; Palmer, P. D.; Rodgers, R. D.; Tait, C. D. *Inorg. Chem.* **1999**, *38*, 1456.
- (19) Panczer, G.; Gaft, M.; Reisfeld, R.; Shoval, S.; Boulon, G.; Champagnon, B. *J. Alloys Comput.* **1998**, *277*, 269.
- (20) Hawkins, H. T.; Spearing, D. R.; Veirs, D. K.; Danis, J. A.; Smith, D. M.; Tait, C. D.; Runde, W. H. *Chem. Mater.* **1999**, *11*, 2851.
- (21) Duff, M. C.; Morris, D. E.; Hunter, D. B.; Bertsch, P. M. *Geochim. Cosmochim. Acta* **2000**, *64*, 1535.
- (22) Hughes, J. M.; Cameron, M.; Crowley, K. D. *Am. Min.* **1989**, *74*, 870.
- (23) Duivenboden, H. C. v.; Ijdo, D. J. W. *Acta Crystallogr.* **1986**, *C42*, 523.
- (24) Ijdo, D. J. W. *Acta Crystallogr. Sec. C* **1993**, *49*, 650.
- (25) Weller, M. T.; Dickens, P. G.; Penny, D. J. *Polyhedron* **1988**, *7*, 243.
- (26) Den Auwer, C.; Simoni, E.; Conradson, S. D.; de Leon, J. M.; Moisy, P.; Beres, A. *C. R. Acad. Sci. Ser. Fascicule C- Chim.* **2000**, *3*, 327.
- (27) Blasse, G. *J. Electrochem. Soc.* **1977**, *124*, 1280.
- (28) Burns, P. C.; Ewing, R. C.; Hawthorne, F. C. *Can. Min.* **1997**, *35*, 1551.
- (29) Rakovan, J. F.; Hughes, J. M. *Can. Min.* **2000**, *38*, 839.
- (30) Luo, S. G.; Li, L. Y.; Tang, B. L.; Wang, D. *Waste Manag.* **1998**, *18*, 55.
- (31) Kuramoto, K.; Mitamura, H.; Banba, T.; Muraoka, S. *Prog. Nucl. Eng.* **1998**, *32*, 509.
- (32) Lumpkin, G. R. *J. Nucl. Mater.* **2001**, *289*, 136.

*Received for review December 21, 2001. Revised manuscript received May 1, 2002. Accepted May 22, 2002.*

ES015874F